Synthesis and Characterization of Mesoporous MCM-48 Containing TiO_2 Nanoparticles

M. Bandyopadhyay, A. Birkner,[†] M. W. E. van den Berg,[‡] K. V. Klementiev,[‡,§] W. Schmidt,[||] W. Grünert,[‡] and H. Gies*

Institute für Geologie, Mineralogie und Geophysik, Lehrstuhl Kristallographie, Lehrstuhl für Physikalische Chemie 1, Lehrstuhl für Technische Chemie, Ruhr-Universität Bochum, Germany, MPI für Kohlenforschung, Mülheim, Germany, and DESY, Hamburg, Germany

Received September 6, 2004. Revised Manuscript Received April 30, 2005

MCM-48 was used as the matrix for size-confined titania. Titanium was introduced into the pores of MCM-48 by wet impregnation using aqueous titanylacetylacetonate, $TiO(acac)_2$, or tetrabutyl orthotitanate in aceton solutions. Calcination in air led to the formation of titania. XRD, TEM, and adsorption investigations confirm the deposition of nanosized particles inside the pores of the mesoporous matrix without destroying their integrity. Chemical analyses show that the titania content increases after successive loading with 14 wt % of Ti after the third impregnation. The structure and size of the particles have been characterized with UV−vis, XANES, and EXAFS spectroscopies. The particle size is 2 nm after the first loading and increases after successive loading, finally showing more than one coordination environment, including resemblance with the structure of bulk rutile-TiO_2. Considering preferential occupation of the channel intersections, this leads to approximately 70% occupancy.

Introduction

The discovery of the novel class of mesoporous M41S materials by Mobil researchers[1,2] opened a new era in the field of porous materials. The wide interest has occurred because of synthesis and application related possibilities which are beyond the original scope of the inventors. The use of a large variety of structure-directing amphiphilic molecules to organize many different metal oxide networks into mesoscopically ordered composite materials has led to new classes of materials.[3] Because of the pore system in the regime between 2 and 100 nm and the periodic arrangement of the pore wall which is amorphous on the atomic scale, they are called ordered mesoporous materials, OMM.[4,5] For the M41S family of materials, the composition is restricted to silicate frameworks, and there are three main mesoporous silicate host structures, MCM-41 (with hexagonal honeycomb symmetry), MCM-48 (with cubic Id3m symmetry), and MCM-50 (a lamellar phase). They have been obtained with diverse amphiphilic surfactants giving a broad range of materials different in unit cell parameters and compositions, however, organized on the basis of the same structural principles.[6]

Because of the narrow pore size distribution and the composition related to zeolites, the materials of the M41S family were first thought to be the geometric extension of the microporous crystalline zeolites into the mesopore regime. Using the silica-based materials, research was focused in the beginning on the exploration of the chemical and physical properties of the mesopore system related to zeolitic properties such as sorption, separation, and catalytic processes. Several reviews about these activities have been reported recently.[7,8]

The catalytically inactive property of the siliceous framework of M41S materials led to many experiments aimed at the substitution of silicon by many metals such as Al, Ti, V, and Ga to introduce active sites. Substitution of Si by Ti created more attention because of the recent success of Ti-substituted zeolites in the catalytic oxidation of various organic molecules. The conventional way to introduce Ti in mesoporous silicas is usually achieved by direct synthesis. Postsynthetic incorporation of Ti in mesoporous silicates is much less investigated; however, some publications are available, for example, on the use of titanium alkoxides[9] or metallocenes.[10] Overall, the postsynthetic incorporation of Ti seems to have a great advantage, that is, the opportunity to start with a highly ordered mesoporous material with a very high inner surface and pore volume.

In addition to the zeolitic applications, the M41S materials are thought to be particularly useful as carriers or matrixes

* Author to whom correspondence should be addressed. E-mail: hermann.gies@rub.de.
[†] Lehrstuhl für Physikalische Chemie 1.
[‡] Lehrstuhl für Technische Chemie.
[§] MPI für Kohlenforschung.
[||] DESY.

(1) Beck, J. S.; Vartuli, J. C.; Roth, W. J.; Leonowicz, M. E.; Kresge, C. T.; Schmitt, K. D.; Higgins, J. L.; Schlenker, J. L. *J. Am. Chem. Soc*. **1992**, *114*, 10834.
(2) Kresge, C. T.; Leonowicz, M. E.; Roth, W. J.; Vartuli, J. C.; Beck, J. S. *Nature* **1992**, *359*, 710.
(3) Lettow, J. S.; Han, Y. J.; Schmidt-Winkel, P.; Yang, P. D.; Zhao, D. Y.; Stucky, G. D.; Ying, J. Y. *Langmuir* **2000**, *16*, 8291.
(4) Raimondi, M. A.; Seddon, J. M. *Liq. Cryst.* **1999**, *26*, 305.
(5) Morey, M. S.; Davidson, A.; Stucky, G. D. *J. Porous Mater*. **1998**, *5*, 195.
(6) Huo, Q. S.; Margolese, D. I.; Cilesla, U.; Feng, P.; Gier, T. E.; Sieger, P.; Leon, R.; Petroff, P. M.; Schüth, F.; Stucky, G. D. *Nature* **1994**, *368*, 317.
(7) Sayari, A. *Chem. Commun*. **1996**, 1840.
(8) Corma, A. *Chem. Rev.* **1997**, 97, *6*, 2373.
(9) Ahn, W. S.; Lee, D. H.; Kim, T. J.; Seo, G.; Ryoo, R. *Appl. Catal., A* **1999**, *181*, 39.
(10) Maschmeyer, T.; Rey, F.; Sankar, G.; Thomas, J. M. *Nature* **1995**, *378*, 159.

10.1021/cm0484854 CCC: $30.25
Published on Web 06/30/2005

for functional molecules or nanoparticles because of their high thermal and chemical stability. Their mesoporous structure could be explored as a host or matrix to immobilize catalytically active species or to provide nanosize confinement inside the pore system.[11−18] In addition, physical, electronic, and sensing properties of other matrix-isolated nanoparticles might be of interest.

Of the materials listed, hexagonal MCM-41, having a one-dimensional array of channel-like pores, is by far the most studied one. This material is easily available and its high reproducibility is achieved with respect to both synthesis and modification. In many papers, various metal oxides such as TiO_2, CdS, ZnO, and SnO_2 have been deposited inside mesoporous MCM-41 to study the physical properties of the nanoparticles inside the mesoporous silica matrix.[19−23] Less attention has been paid to the cubic MCM-48 type materials.[2] This is also true for SBA-type,[24,25] STA-type,[26,27] and other mesoporous silicate based materials,[28,29] which have been synthesized meanwhile.

In particular, MCM-48-type materials might have several advantages over, for example, MCM-41. The cubic symmetry of MCM-48 with its three-dimensional framework periodicity and the set of two, interpenetrating, three-dimensional pore systems makes it very special. Compared to one- or two-dimensional pore systems, the three-dimensional pore system has more resistance against pore blockage and provides a more efficient diffusion pathway.

In previous studies, we have explored the use of MCM-48 as a matrix for metal oxides with catalytic activity such as ZnO, CuO, and Cu/ZnO.[18,21] Here, we report on the deposition of Ti salts within the pore system of cubic MCM-48 and their subsequent decomposition to Ti-oxides clusters. The final product underwent thorough characterization by means of X-ray powder diffraction, N_2 adsorption, IR-spectroscopy, ICP AES analysis, and UV−visible, EXAFS, and XANES spectroscopies along with TEM. Similar to previous studies for zeolites,[30] we have tried to combine all these characterization methods to come to a consistent conclusion about the structure, the properties, the location, and the coordination state of Ti in TiO_2 in Ti-impregnated MCM-48 material.

Experimental Section

Synthesis of MCM-48. Pure silica MCM-48 was synthesized following the method described by Gies et al.[18] In a typical synthesis, cetyltrimethylammonium chloride (CTACl, Aldrich, 25% aqueous solution) was added to 1 M NaOH in polypropylene bottles under continuous stirring followed by the addition of tetraethyl orthosilicate (TEOS, Merck) to give a final molar composition of $NaOH:H_2O:CTACl:TEOS = 0.5:64:0.7:1$. Finally, the homogeneous gel was heated at 90 °C for 4 days. After that, the solid sample was filtered, washed with water, and dried overnight at room temperature. The dried product was calcined at 540 °C for 5 h (heating rate1 K/min)

Impregnation. So far, Ti has been incorporated in MCM-48 either by grafting or addition of the metal ion during the synthesis.[31−34] Other than for MCM-41, the postsynthetic wet-impregnation method has not been utilized yet for MCM-48, and the thorough exploration of this method is investigated in the present study. Two different Ti sources, titanylacetylacetonate ($TiO(acac)_2$, Merck) and tetrabutyl orthotitanate (Merck), were used for the impregnation. During the impregnation with titanylacetylacetonate, an appropriate amount of $TiO(acac)_2$ was dissolved in water (0.01 M). The impregnation of the calcined and dried MCM-48 (0.6 g) was carried out by stirring the sample for 2 h with the aqueous $TiO(acac)_2$ solution (200 mL). The mixture was then filtered and washed thoroughly with water and dried at room temperature overnight. The thermal decomposition of the metal acetylacetonate was carried out in a calcination oven in air by heating the sample at 300 °C for 5 h.

On the other hand, for the impregnation with tetrabutyl orthotitanate, the standard MCM-48, which was dried overnight in vacuum at 180 °C, was reacted with a solution of this Ti source in dry acetone (0.05 m). The mixture was stirred for 6 h at room temperature. As tetrabutyl orthotitanate is moisture-sensitive, the whole procedure was carried out in dry N_2 atmosphere. Finally, the solid was filtered off carefully, washed with acetone, dried at room temperature, and then calcined at 300 °C for 5 h. For successive impregnations, the respective procedure was repeated several times.

Characterization of the Synthesis Product

XRD. X-ray powder diffraction experiments were carried out using a Philips diffractometer with Cu Kα radiation ($\lambda = 1.5418$ Å) in Bragg−Brentano geometry on flat plate sample holders. For long exposure times, a Siemens D5000 diffractometer was used

(11) Köhn, R.; Fröba, M. *Catal. Today* **2001**, *68*, 227.
(12) Morey, M.; Davidson, A.; Stucky, G. *Microporous Mater*. **1996**, *6*, 1996.
(13) Koyano, K. A.; Tatsumi, T. *Chem. Commun*. **1996**, 145.
(14) Corma, A.; Kan, Q.; Rey, F. *Chem. Commun*. **1998**, 579.
(15) Walker, J. V.; Morey, M.; Carlsson, H.; Davidson, A.; Stucky, G. D.; Butler, A. *J. Am. Chem. Soc*. **1997**, *119*, 6921.
(16) Morey, M.; Davidson, A.; Eckert, H.; Stucky, G. D. *Chem. Mater*. **1996**, *8*, 486.
(17) Kawi, S.; Te, M. *Catal. Today* **1998**, *44*, 101.
(18) Gies, H.; Grabowski, S.; Bandyopadhyay, M.; Grünert, W.; Tkachenko, O. P.; Klementiev, K. V.; Birkner, A. *Microporous Mesoporous Mater*. **2003**, *60*, 31.
(19) Trong On, D.; Desplantier-Giscard, D.; Danumah, C.; Kaliaguine, S. *Appl. Catal., A* **2001**, *222*, 299.
(20) Wellmann, H.; Rathousky, J.; Wark, M.; Zukal, A.; Schulz-Ekloff, G. *Microporous Mesoporous Mater*. **2001**, *44*, 419.
(21) Tkachenko, O. P.; Klementiev, K. V.; Löffler, E.; Ritzkopf, I.; Schüth, F.; Bandyopadhyay, M.; Grabowski, S.; Gies, H.; Hagen, V.; Muhler, M.; Lianhai, L.; Fischer, R. A.; Grünert, W. *Phys. Chem. Chem. Phys.* **2003**, *5*, 4325.
(22) Wark, M.; Rohlfing, Y.; Altindag, Y.; Wellmann, H. *Phys. Chem. Chem. Phys*. **2003**, *5*, 5188.
(23) Uphade, B. S.; Akita, T.; Nakamura, T.; Haruta, M. *J. Catal*. **2002**, *209*, 331.
(24) Huo, Q.; Leon, R.; Petrov, P. M.; Stucky, G. D. *Science* **1995**, *268*, 1324.
(25) Huo, Q. S.; Margolese, D. I.; Stucky, G. D. *Chem. Mater*. **1996**, *8*, 1147.
(26) Noble, G. W.; Wright, P. A.; Lightfoot, P.; Morris, R. E.; Hudson, K. J.; Kvick, A.; Graafsma, H. *Angew. Chem., Int. Ed. Engl*. **1997**, *36*, 81.
(27) Garcia, R.; Philp, E. F.; Slawin, A. M. Z.; Wright, P. A. *J. Mater. Chem*. **2001**, *11*, 1421.
(28) Tanev, P. T.; Pinnavaia, T. J. *Science* **1995**, *279*, 548.
(29) Inagaki, S.; Fukushima, Y.; Kuroda, K. In *Zeolites and Related Microporous Materials: State of the Art 1994*; Weitkamp, J., Karge, H. G., Pfeifer, H., Hölderich, W., Eds.; Studies in Surface Science and Catalysis; Elsevier: Amsterdam, 1994; Vol. 84, Part A, p 125.
(30) Grubert, G.; Stockenhuber, M.; Tkachenko, O. P.; Wark, M. *Chem. Mater* **2002**, *16*, 2458.
(31) Blasco, T.; Corma, A.; Navarro, M. T.; Perez-Pariente, J. *J. Catal*. **1995**, *65*, 156.
(32) Chen, Y. W.; Lin, H. Y. *J. Porous Mater*. **2002**, *9*, 175.
(33) Ahn, W. S.; Kim, N. K.; Jeong, S. Y. *Catal. Today* **2001**, *68*, 83.
(34) Schrijnemakers, K.; Vansant, E. F. *J. Porous Mater*. **2001**, *8*, 83.

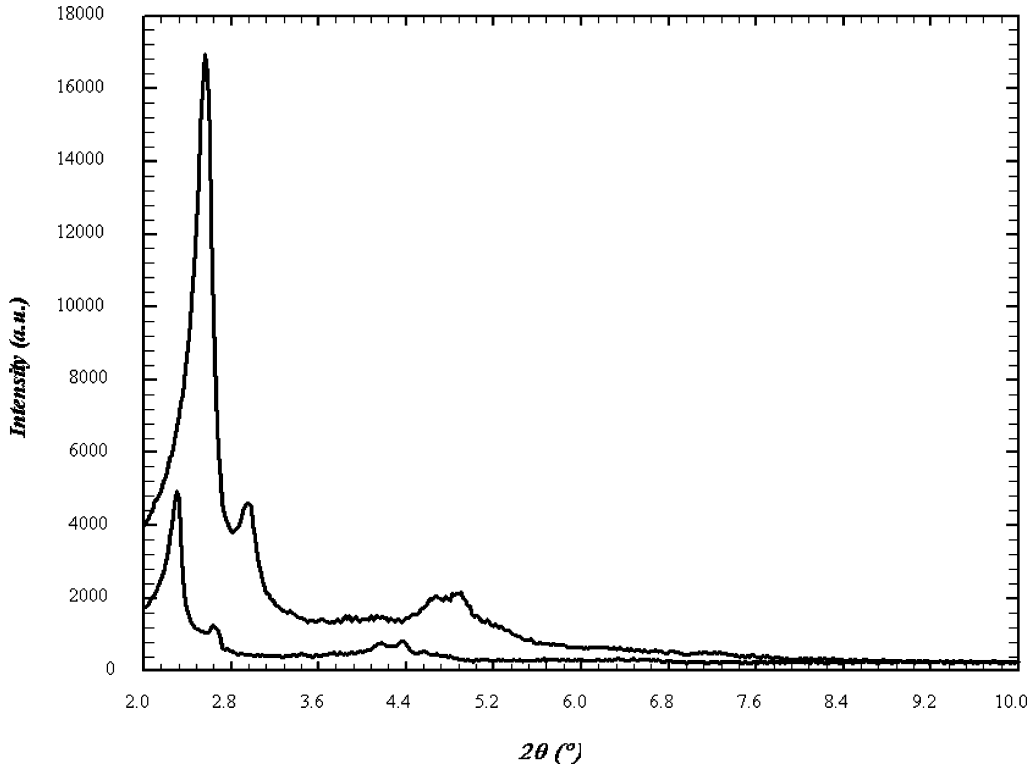

Figure 1. XRD diagram of as-synthesized and calcined MCM-48. The well-ordered structure of the silica matrix shows up in sharp reflections up to rather high diffraction angles.

operating in transmission mode (modified Debye Scherrer geometry) with monochromatized Cu $K\alpha_1$ radiation. The sample was loaded in a glass capillary.

Physisorption. The nitrogen adsorption measurements were performed on a ASAP 2010 unit (Micromeritics). For the analysis of the data applying the nonlocal density functional theory (NLDFT) method, the data were processed using the Autosorb software package provided by Quantachrome. Prior to the sorption experiment, the materials were dehydrated by evacuation under specific conditions (250 °C, 10 h). Since the adsorption and desorption branches of the isotherms showed no hysteresis at pressures in the range of the capillary condensation, the pore size distributions were derived by using the NLDFT equilibrium model for nitrogen adsorption on oxidic surfaces. The pore size distribution calculation according to the BJH theory resulted in mean pore diameter being about 1 nm too small.[35]

Transmission Electron Microscopy. A Hitachi H-8100 scanning and transmission electron microscope operating at accelerating voltages up to 200 kV with a single-crystal LaB_6 filament was used for the TEM studies. The specimens were prepared by placing a drop of the dilute solution of the calcined powder samples in ethanol on a carbon-coated copper grid. The samples were allowed to dry at room temperature.

UV−Visible Spectroscopy. UV−visible spectra were recorded on a Perkin-Elmer Lamda 9 UV/Vis/NIR spectrophotometer equipped with an RSA-PE-19 biconical optical bench for diffuse reflectance measurement. All samples were measured with $BaSO_4$ as reference.

Inductively Coupled Plasma Atomic Emission Spectroscopy (ICP AES). The chemical composition of the samples was determined by ICP AES. The samples were fused with Na_2O_2, dissolved in water, and neutralized with HNO_3. The analyses were performed using ICP-AES spectrometer (PU 7000, Philips).

EXAFS and XANES Spectra. X-ray absorption spectra (Ti K edge at 4966.0 eV) were measured at the Hasylab E4 station (DESY, Hamburg, Germany). This beamline was equipped with a Si(111) double-crystal monochromator that was used to detune to 50% of the maximum intensity to exclude higher harmonics present in the X-ray beam. The samples were mixed with polyethylene and were pressed into wafers of sufficient thickness. The spectra μ(E) were measured in transmission mode using ionization chambers, with the sample wafer at liquid nitrogen temperature. A titanium metal foil (between the second and the third ionization chamber) was measured at the same time for energy calibration purposes. Data treatment was carried out using the software package VIPER.[36] For background subtraction, a Victoreen polynomial was fitted to the preedge region. A smooth atomic background, μ_0(k), was evaluated using smoothed cubic splines. The radial distribution function FT$[k^2\chi(k)]$ was obtained by Fourier transformation of the k^2-weighted experimental function $\chi(k) = (\mu(k) - \mu_0(k))/\mu_0(k)$ multiplied by a Bessel window. For the determination of structural parameters, theoretical references calculated by the FEFF8.10 code[37] were used. To minimize the number of free parameters, equal backscatters were fitted with the same E_0-shift whenever possible (variations of ±1 eV permitted). The edge region was measured with an energy step of 0.1 eV. Duplicate spectra were recorded to ensure data reproducibility.

Results and Discussion

MCM-48 which was synthesized by the hydrothermal method was well periodically ordered. The XRD patterns of a well-ordered, as-synthesized, and calcined MCM-48 as well as those for average samples with slightly broader

(35) Ciesla, U.; Schüth, F. *Microporous Mesoporous Mater*. **1999**, *27*, 131.

(36) Klementiev, K. V. VIPER for Windows (Visual Processing in EXAFS Researches), freeware, available from <www.desy.de/~klmn/viper.html>.

(37) Ankudinov, A. L.; Ravel, B.; Rehr, J. J.; Conradson, S. D. *Phys. Rev.* **1998**, *B58*, 7565.

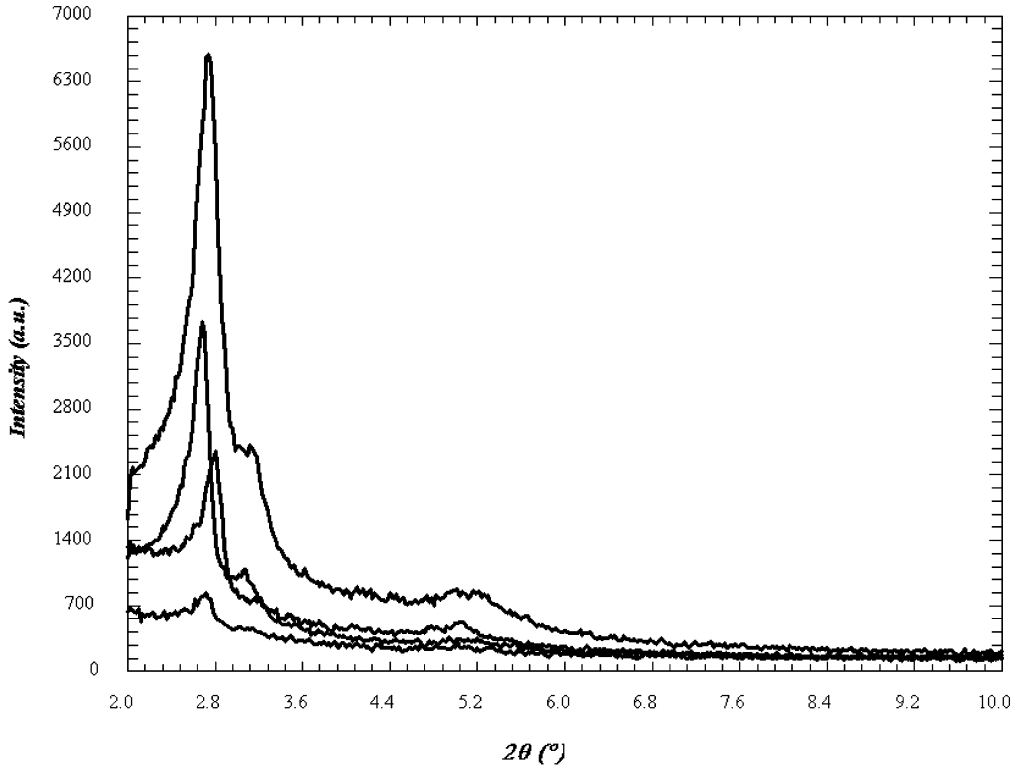

Figure 2. XRD diagrams of calcined MCM-48 and successive Ti-impregnated MCM-48. (a) Calcined MCM-48, (b) first Ti-impregnated MCM-48, (c) second Ti-impregnated MCM-48, and (d) third Ti-impregnated MCM-48. The decrease in peak intensities is related to the loss in diffraction contrast between wall and pore.

Table 1. Summary of Characteristic Crystallographic Properties of Calcined MCM-41

lattice parameter	83.88 Å (calcined)
cell volume	590,168 $Å^3$ (calcined)
space group symmetry	*Ia3d*
number of channel intersections	16
number of diffraction peaks resolved	6
peak fwhm (first peak)	0.2° 2θ

diffraction signals loaded with increasing amounts of titania are given in Figures 1 and 2, respectively. Table 1 lists the characteristic crystallographic data of the material. The (2 2 0) peak at around 2.8° 2θ was present for all materials even after the second and third loading with titania. This confirms that after the impregnation procedure the structure of the silica matrix is well maintained. From systematic studies of the influence of the sorbate on the intensity of the diffraction peaks, it is known that the uptake of molecules inside the pores reduces the scattering contrast between pore wall and pore thus leading to a decrease in peak intensity.[38] The higher the electron density of the sorbate molecule, the lower the residual peak intensity in the powder diffraction diagram is. This is clearly reflected in the diffraction diagrams of the titania-loaded samples in Figure 2. However, the decrease of peak intensity with successive loading of metal salt may also be due to loss of sample integrity. To rule out the degradation of the sample and to confirm the interpretation of the XRD experiments, complementary TEM studies were carried out. The integrity of every sample was checked with TEM together with its qualitative titania content using EDX. The results of the analyses always showed the well-ordered and well-maintained silica host structure, no external titania particles, and a well-resolved EDX titanium signal from material deposited inside the pores.

The impregnation of dried MCM-48 samples was carried out in aqueous solution for $TiO(acac)_2$ and in dry aceton for tetrabutyl orthotitanate as titanium sources. After the removal of the solvent, the thermal decomposition of the sorbate molecules at 300 °C in air led to the formation of titania inside the pores of the MCM-48 matrix. To check for titania deposited on the external surface of the silica matrix, powder XRD diagrams with Cu Kα radiation of all the materials were recorded up to 2θ of 50°. No additional diffraction peak was observed at higher angles in regular step scan mode and step counting times of 5 s. In addition, diffraction experiments were carried out using a position-sensitive detector and 36-h exposure time to detect minor amounts of titania nanoparticles in the sample after the third loading. In the range from 20 to 35° 2θ, in which the major peaks of the three crystalline polymorphs rutile, anatase, and brookite are found, no additional diffraction intensities were recorded which could be unambiguously attributed to crystalline titania. These experiments support the conclusion that no titania has been deposited on the outer surface with particle size above 3 nm and that the size confinement of the MCM-48 matrix has led to the formation of titania particles of size less than the MCM-48 pore diameter, that is, ~3 nm diameter inside the pores. On the basis of the Scherrer formula, the peak half-width for such small crystalline particles would be more than 4°. Therefore, the diffraction experiment in the range measured shows a superposition of the contribution of the amorphous glass of the capillary and the MCM-48 matrix together with a possible broad contribution of the titania nanoparticles.

(38) Marler, B.; Oberhagemann, U.; Vortmann, S.; Gies, H. *Microporous Mater.* **1996**, *6*, 375.

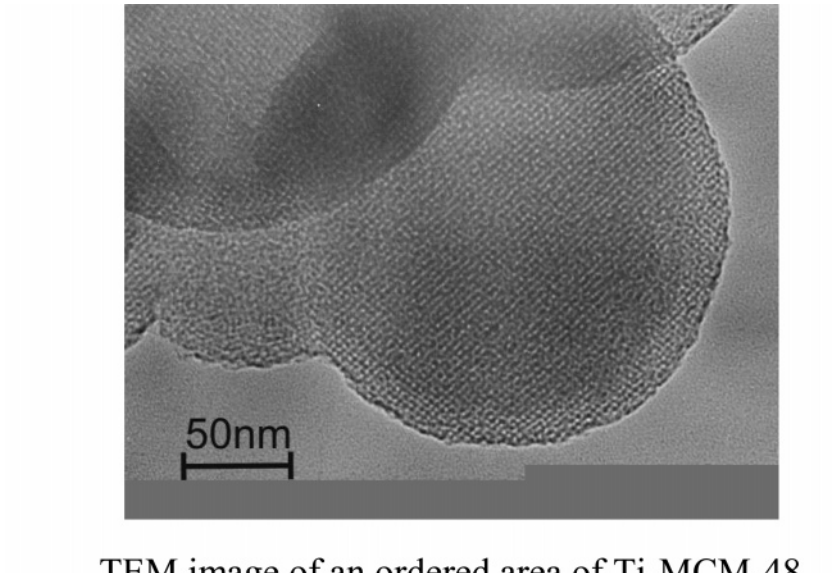

Figure 3. TEM image of a MCM-48 particle impregnated with Ti using titanylacetylacetonate together with the corresponding EDX spectrum. The TEM image shows the regular structure of MCM-48, and the TiK_α and TiK_β signals in the EDX spectrum indicate that the incorporation of Ti into the silicate framework has been successful.

Table 2. Results of the Chemical and EXAFS Ti Analyses

sample	chemical analysis	EXAFS analysis
Ti-MCM-48(1)	13 wt %	7 wt %
Ti-MCM-48(2)	14 wt %	10 wt %
Ti-MCM-48(3)	16 wt %	12 wt %

The Ti content of the impregnated samples was determined from EXAFS measurements and ICP AES analyses (Table 2). Within the experimental uncertainty, the results of the analyses are in agreement with approximately 14 wt % Ti after the third loading.

In Figure 3a, a TEM image of a well-aligned MCM-48 particle after Ti-impregnation using titanylacetylacetonate as Ti source is shown together with the EDX analysis. The lattice fringes of this well-ordered crystallite have a d spacing of $d \sim 3.2$ nm corresponding to (110) planes. The regular contrast variation in the TEM image shows the intact MCM-48 silicate framework. For all imaged MCM-48 particles, no damage of the periodic structure of the silicate framework was observed. It is concluded that the impregnation procedure and the consecutive thermal treatment does not damage the MCM-48 silica host framework. In the course of the TEM measurements of a large number of isolated MCM-48 particles as well as aggregates, we have not observed any large TiO_2 particles situated outside of the silicate framework which might be responsible for the Ti signals in the EDX spectrum. The EDX spectrum in Figure 3 shows the O Kα and Si Kα signals from the silicate framework as well as the Ti Kα and Ti Kβ signals resulting from the Ti-impregnation of the calcined MCM-48 sample. The C Kα signal in the EDX spectrum results from sample contamination during the TEM and EDX measurements, and the Cu signals in this spectrum are caused by the copper grid for sample preparation. The TEM and EDX results indicate that Ti is incor-

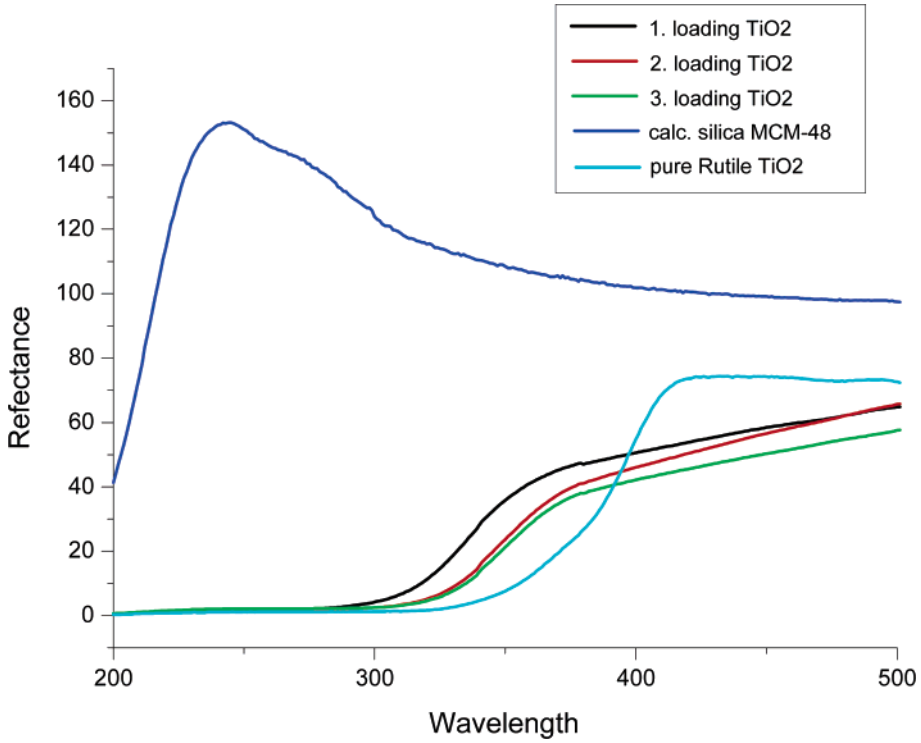

Figure 4. UV−visible spectra in reflectance mode of pure rutile, silica MCM-48, and MCM-48 after successive impregnation with tetrabutyl orthotitanate showing the blue shift of the signal because of nanosized TiO_2 particles.

porated inside MCM-48 using titanylacetylacetonate or tetrabutyl orthotitanite as the Ti source. However, no isolated titania particles inside the MCM-matrix could be resolved and analyzed in the TEM experiments. Selected area electron diffraction experiments (SAED) of well-resolved parts of MCM-48 loaded with titania were not conclusive.

Adsorption isotherms are used as a macroscopic average measurement for exploring the surface area, the pore diameter, and the volume of the samples. Table 3 summarizes the measurements of the different MCM-48 samples without and with titania. Using the NLDFT method for the analysis of the isotherms, the surface area of calcined MCM-48 was determined to be 813 m^2/g with 3.3-nm pore diameter and 0.77 cm^3/g pore volume. This is in agreement with data published in the literature[39] and confirms the good quality of the MCM-48 sample. The successive loading of titania leads to a stepwise decrease of the pore volume (0.45 cm^3 m^3/g) and a decrease of the average pore diameter (28 Å). However, in addition to the mesopores, micropores have also been observed with ~10 Å pore diameter in the titania-loaded samples. This might indicate that the pore wall degrades and becomes more and more porous or that the formation of titania particles inside the MCM-48 channels leads to micropores between the silica wall and the titania or between titania particles. The fact that the micropore diameter decreases only little supports the formation of particles, since the creation of pores in the silica wall should lead to further widening of the micropore diameter at successive loading as the corrosion process proceeds. Surprisingly, the surface area even after the second impregnation is almost unchanged. Only after the third impregnation has a significant decrease of surface area to 618 m^2/g been measured. Normalized to 1 g silica MCM-48, this relates to 760 m^2/g. This finding has been confirmed by several measurements, also using the BJH approach for the interpretation of the isotherms. The results of the surface measurements in combination with the development of the pore volume are in agreement with the formation of particles inside the pores which reduce the pore volume continuously, however, creating additional surface area for low loadings, for example, through surface roughening. Only after considerable loading of titania do the coverage and blockage of the surface area of the matrix outweigh the contribution of the newly created surface by the titania particles. Similar observations have already been reported by Wark et al. for titania in MCM-41, however, without detailed discussion.[40]

UV−vis spectra of Ti-containing mesoporous materials are usually characterized by broad absorption bands appearing at 220 and 260−270 nm.[33,41] The band at 220 nm could be associated with isolated Ti in the framework, which is similar in character to that in TS-1[42] and Ti-Beta.[43] This band has been assigned to the Ti atoms in octahedral coordination, in which two water molecules form part of the metal coordination sphere. The band at 270 nm could be due to the presence of partially polymerized hexacoordinated Ti species,[42] however, Ti−O−Ti clusters can also exist along with the isolated Ti sites to some extent. The UV−vis reflectance spectra of calcined TiO_2/MCM-48 are given in

(39) Ravikovitch, P. I.; Wei, D.; Chueh, W. T.; Haller, G. L.; Neimark, A. V. *J. Phys. Chem. B* **1997**, *101*, 3671.
(40) Prochnow, P.; Schulz-Ekloff, G.; Wark, M.; Thomas, J. K.; Zukal, A.; Rathousky, J. *Proceedings of the 13th International Zeolite Conference*; Garlaneau, A., di Renzo, F., Fajula, F., Vedrine, J., Eds.; *Stud. Surf. Sci. Catal.* **2001**, *135*, 359.
(41) Zhang, W.; Fröba, M.; Wang, J.; Tanev, P. T.; Wong, J.; Pinnavaia, T. J. *J. Am. Chem. Soc.* **1996**, *118*, 9164.
(42) Petrini, G.; Cesana, A.; De Alberti, G.; Genoni, F.; Leofanti, G.; Padovan, M.; Paparatto, G.; Rofia, P. *Stud. Surf. Sci. Catal*. **1991**, *68*, 761.
(43) Camblor, M. A.; Corma, A.; Martinez, A. *J. Chem. Soc., Chem. Commun*. **1992**, 589.

Table 3. Results of Nitrogen Adsorption Measurements of a Calcined Reference MCM-48 and Different Ti Impregnated MCM-48

sample	pore diameter (Å)	pore volume (cm^3/g)	surface area (m^2/g)
MCM-48	33	0.77	813
Ti-MCM-48 (2)	32	0.66	880
Ti-MCM-48 (3)	28	0.45	618

Figure 4. The absence of a broad absorption band at around 370 nm confirms the absence of large TiO_2 crystals in TiO_2/MCM-48 material which would be related to titania particles deposited on the external surface. The reflectance spectra of TiO_2/MCM-48 are also compared with the one of pure rutile-TiO_2. A clear shift of the absorption by ~30 nm in the TiO_2/MCM-48 sample after the first loading toward lower wavelength is observed. This is an indication of a particle size effect on the absorption energy. For nanoparticles in the quantum dot range, the frequency shifts toward lower wavelength with the decrease of the particle diameter. The pores of MCM-48 provide a size confinement for titania with a maximum particle size of ~3 nm for which a blue shift in the absorption of titania is expected. This feature is clearly reflected here. The energy shifts toward higher wavelength with increasing metal content indicate a particle size increase. Considering the energy shift of approximately 1700 cm^{-1} and using the formalism described by Kormann et al.,[44] a particle size of ~2 nm in diameter is calculated which is in perfect agreement with the pore confinement by the MCM-48 matrix.

On the basis of a particle size of ~2 nm, the crystallographic data of MCM-48, and the density of calcined MCM-48 of ~0.97 g/cm^3, the distribution of nanoparticles inside MCM-48 has been calculated. Assuming that the deposition occurs preferentially at the channel intersection for the three-times loaded sample with 14 wt % Ti, ~70% occupancy of the channel intersection has been calculated. Since the void space at the intersection is at least 3 nm in diameter as Terasaki[45] has shown experimentally from electron diffraction structure analysis for MCM-48, micropores are created, still allowing for the three-dimensional diffusion without pore blockage.

The local environment around Ti was studied through XAS spectra at the Ti K edge (4966 eV). In Figure 5, the XANES spectra of Ti loaded samples are compared with those of the reference oxides rutile and anatase. It can be seen that the scattering features above the edge are much less distinct in the TiO_2/MCM-48 materials than in the reference oxides, which indicates a less ordered structure. Closer inspection shows that the sequence of scattering features is completely different from that in anatase while it is reminiscent of that in rutile. This suggests that the short-range order of the TiO_2 entities is closer to rutile than to anatase.

The discussion of Ti XAFS spectra is often focused on the distinctive preedge peak,[46−49] the normalized peak height

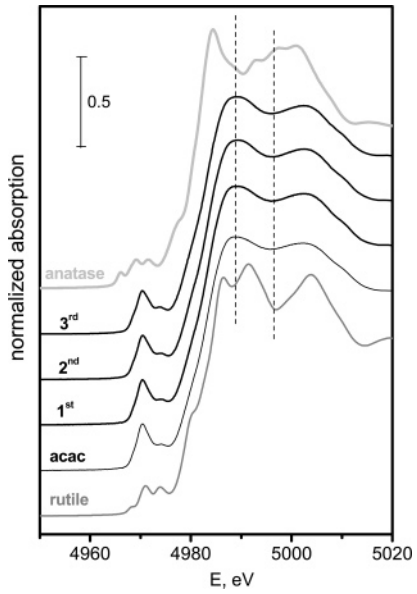

Figure 5. Ti K edge XANES spectra of calcined TiO_2/MCM-48 samples and reference materials, showing normalized absorption versus energy.

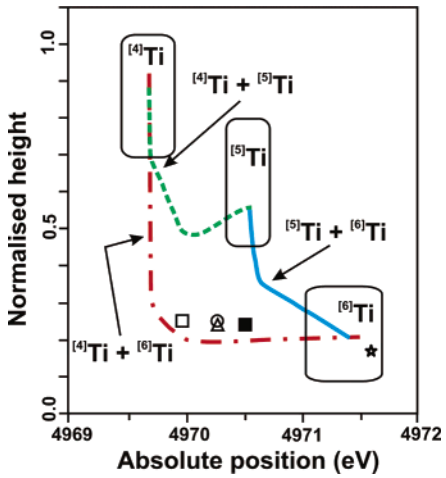

Figure 6. Relation between the absolute position and the height of the Ti preedge feature for Ti containing standard compounds. After Farges et al.[37] areas are showing coordination of the central Ti atom; lines indicate mixtures of compounds, where the arrows indicate a 1:1 ratio between compounds. Symbols represent samples measured for this work. (□) Acetylacetonate precursor, (○) first impregnation, (△) second impregnation, (■) third impregnation, and (★) rutile.

of which is ~0.25 in the case of the TiO_2/MCM-48 samples under investigation. The energy position of the preedge peak lies around 4970.3 eV (vide Table 2). Farges et al. have conducted an extensive study of position and height of this preedge peak using titanium-containing reference compounds.[46] They constructed a profile of normalized peak height versus its absolute position and defined three regions corresponding to 4-, 5-, and 6-fold coordinated Ti, which have been summarized in Figure 6. Samples measured for the present work are included in this figure as well. From this, the intraporous titania entities should contain Ti atoms in both 4- and 6-coordinated environments, the latter being

(44) Kormann, C.; Bahnemann, D. W.; Hoffmann, M. R. *J. Phys. Chem.* **1988**, *92*, 5196.
(45) Kaneda, M.; Tsubakiyama, T.; Carlsson, A.; Sakamoto, Y.; Ohsuna, T.; Terasaki, O. *J. Phys. Chem. B* **2002**, *106*, 1256.
(46) Farges, F.; Brown, G. E.; Rehr, J. J. *Phys. Rev.* **1997**, *B 56*, 1809.
(47) Davis, R. J.; Liu, Z.; Tabora, J. E.; Wieland, W. S. *Catal. Lett.* **1995**, *34*, 101.
(48) Sankar, G.; Thomas, J. M.; Richard, C.; Catlow, A. *Top. Catal.* **2000**, *10*, 255.
(49) Yoshitake, H.; Sugihara, T.; Tatsumi, T. *Phys. Chem. Chem. Phys.* **2003**, *5*, 767.

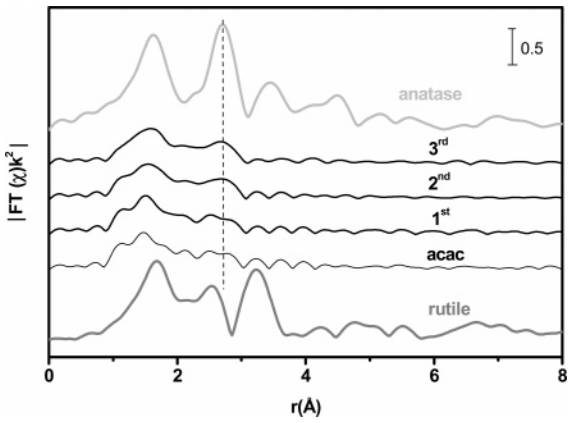

Figure 7. Fourier transform Ti K edge EXAFS spectra ($5.1 < k < 15.8$ $Å^{-1}$) of calcined TiO_2/MCM-48 samples and reference materials.

increasingly predominant with increasing Ti loading. However, the basis of this assignment is empirical. In fact, Farges et al. supported their findings by calculations using FEFF6 and FEFF7 codes. Although this is an often-used tool for calculating EXAFS spectra, we believe that it is not suited to accurately predict the shape of the features around the edge (XANES region), especially to model preedge peaks.

In Figure 7, the TiK-EXAFS spectra of the Ti-loaded MCM-48 samples are compared with those of the rutile and anatase reference oxides. The analysis of the spectra confirms that the titania entities formed are highly disordered and are most likely very small: The scattering features are much less intense than those in the reference oxides, and no scattering features can be discerned above 3.5 Å (uncorrected). The radial distributions of the scattered intensity resemble that of rutile in particular after the second and third impregnation, where significant scattering intensity is found between the features at 1.6 and 2.6 Å (uncorrected) unlike the spectrum of anatase. This agrees with observations made in the XANES region. Closer inspection shows, however, that the feature near 3 Å (uncorrected) appears at the position

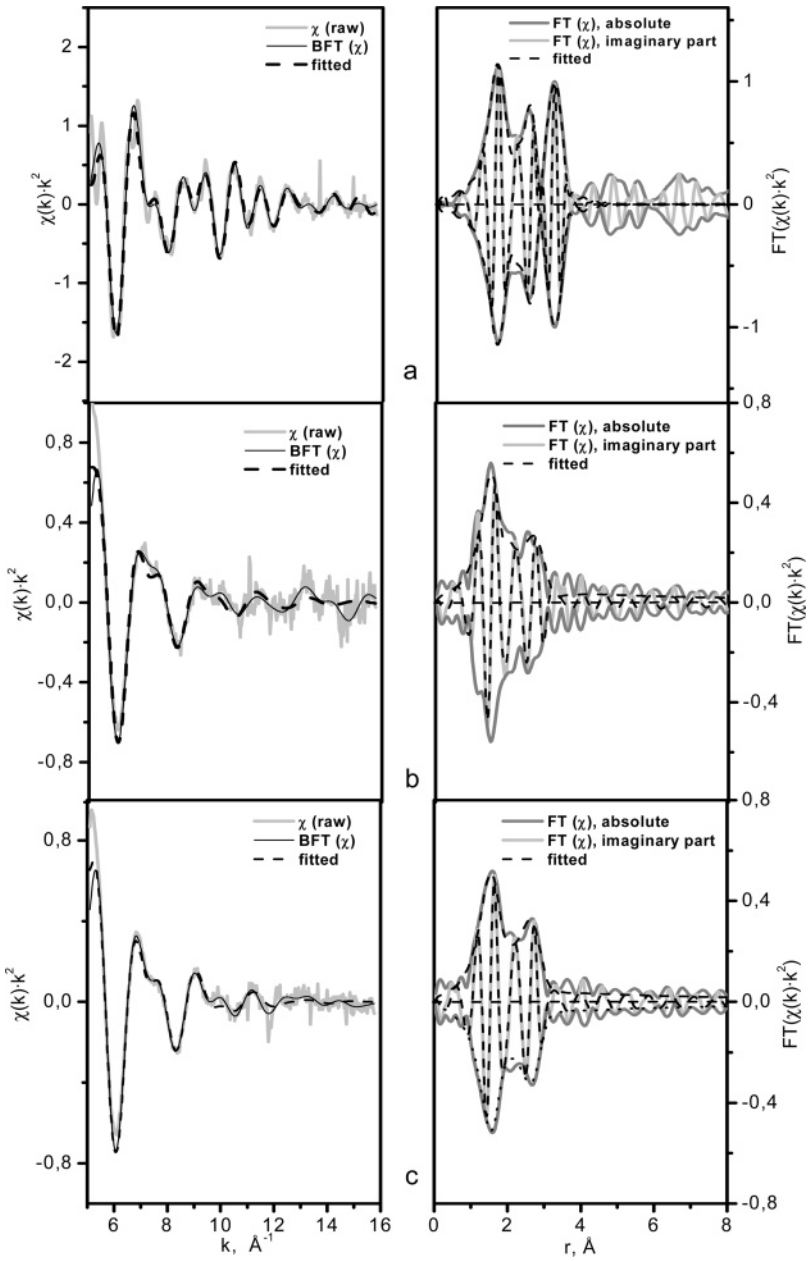

Figure 8. EXAFS spectra of titanium samples in k^2 space (left) and in r-space (right). Top: rutile. Middle: once impregnated. Bottom: three times impregnated.

Table 4. Peak Data for the Preedge Feature Found in the XAS Spectra of TiO_2/MCM-48

sample	corrected preedge position[a]	shift relative to Ti foil[b]	normalized preedge height[c]
acac	4970.0	3.2	0.26
first impregnation	4970.3	3.5	0.25
second impregnation	4970.3	3.5	0.24
third impregnation	4970.5	3.7	0.24
rutile	4971.6	4.8	0.17
rutile[45]	4971.6	not given	0.22

[a] Corrected with respect to the position of the preedge feature of the Ti reference foil and to the literature value for rutile. [b] Shift relative to the position of the preedge feature in the Ti reference foil. [c] Normalized to the absorption edge height.

Table 5. Model Parameters of EXAFS Fits—Rutile Reference and TiO_x/MCM-48, First and Third Impregnation (See Figure 8)

no.	element	R, Å	C. N.[a]	$10^3\,\sigma^2$, Å^{-2}	E_0, eV
		Rutile (Figure 10a)			
1	O	1.935 ± 0.013 (1.948)[b]	4	7.3 ± 1.8	6.7
2	O	1.983 ± 0.020 (1.980)[b]	2	4.6 ± 2.5	6.7
3	Ti	2.9783 ± 0.015 (2.959)[b]	2	3.6 ± 1.5	4.5
4	Ti−O[c]	3.48 ± 0.1 (3.428)[b]	8	4 ± 15	4.5
5	O	3.521 ± 0.035 (3.487)[b]	4	2.6 ± 3.7	6.2
6	O	3.547 ± 0.032 (3.560)[b]	4	2.0 ± 3.1	5.0
7	Ti	3.531 ± 0.013 (3.569)[b]	8	8.6 ± 1.7	5.0
		TiO_x/MCM-48, first impregnation (Figure 10b)			
1	O	1.876 ± 0.005	4.1 ± 0.2	8.7 ± 0.7	7.0
2	O	2.052 ± 0.014	1.0 ± 0.2	4.5 ± 1.7	6.4
3	Ti	3.110 ± 0.015	3.4 ± 0.6	17.5 ± 2.4	14.2
		TiO_x/MCM-48, third impregnation (Figure 10c)			
1	O	1.880 ± 0.004	4.1 ± 0.2	11.0 ± 0.6	5.0
2	O	2.006 ± 0.021	1.2 ± 0.3	14.2 ± 3.3	5.0
3	Ti	3.051 ± 0.008	3.5 ± 0.4	14.7 ± 1.2	6.5

[a] Fixed to crystallographic values according to ref 52. [b] According to ref 52. [c] Multiple scattering path.

expected for anatase rather than at that for rutile (indicated by the broken line); in fact, in some of the spectra this feature appears to be split into two weak maxima. This indicates that the short-range order is not identical to that of rutile or that more than one type of coordination spheres is present.

To extract more detailed information about the coordination environment in our samples, representative EXAFS spectra were fitted to structural models. Results of this fitting procedure (bond lengths, coordination numbers, Debye−Waller factors, and edge-shift corrections) are reported in Table 5. To validate the data reduction procedures adopted and the FEFF parameters used, the EXAFS spectrum of rutile was fitted first. A satisfactory fit of the rutile spectrum beyond the first oxygen sphere as given in Figure 8a and Table 5 was possible only when the k range used was cut at the rather high value of ca. 5 Å^{-1} (actual range $5.1 < k < 15.8$ Å^{-1}). This is obviously due to intense multielectron excitations near the Ti K edge,[46] which distorts the signal at low k values also in the EXAFS region and is therefore a general problem of EXAFS at the Ti K edge although it does not seem to have received much attention in earlier model calculations.[30,50,51] The ab initio XAFS code FEFF considers multielectron excitations as an integral amplitude-damping effect, without particular energy dependence, which in some cases leads to inadequate EXAFS amplitude at small k values. Only with the limitation to the k range mentioned above did the EXAFS spectrum of rutile correlate with the rutile crystal structure and did the spectra of the TiO_2/MCM-48 sample attain a shape that permitted an interpretation consistent with the observations in the XANES region.

The spectra of the TiO_2−MCM-48 samples could be modeled with two oxygen and one titanium shell as in the rutile structure but at different distances (Table 5, Figure 8b, c). For the sample after the third impregnation, alternative models were tested, for example, with a third oxygen shell instead of a titanium one, but they reproduced the spectrum less accurately. This supports that the TiO_2 entities have, indeed, formed clustered structures. These clusters are highly defective as shown by the sometimes very high Debye−Waller factors (static disorder) and also by the lower sum of the O coordination numbers (C. N.), which was smaller in the aggregates deposited into MCM-48 than with rutile (Figure 5.1−5.3 vs 6). Despite some differences in the shape of the Fourier transformed spectrum,[7] the models for the samples after the first and the third impregnation are rather similar. When more titania is deposited, some shifts in the shell distances can be seen which tend toward the values of rutile. Analogously, the sum of coordination numbers of the two oxygen shells increases slightly. It has to be admitted that this increase is hardly significant with the given error limits of the method; however, it agrees with an analogous conclusion drawn from the XANES region (vide supra, Figure 6). An increase of the particle size as indicated by the UV spectra cannot be inferred from the EXAFS spectra. This is, however, not unexpected because of the highly disordered nature of the TiO_2 phase.

In summary, we demonstrate the formation of TiO_2 nanoclusters in the pore system of MCM-48. The material has been used to prepare highly active catalysts for CO oxidation by additional deposition of Au nanoparticles into the pores.[53] Other applications in catalysis, photocatalysis, sensorics, and so forth may be envisaged.

Conclusion

A simple and effective wet impregnation method was applied for the incorporation of Ti in siliceous MCM-48, which yielded highly ordered mesoporous material with high surface area. The decrease of intensity, reflected in the X-ray diffraction diagram, with successive loading by metal oxide directly proves the uptake of titania inside the pore system. The regular contrast variation in the TEM image shows the intact MCM-48 silicate framework, and the EDX spectra

(50) Gleeson, D.; Sankar, S.; Catlow, C. R. A.; Thomas, J. M.; Spanó, G.; Bordiga, S.; Zecchina, A.; Lamberti, C. *Phys. Chem. Chem. Phys.* **2000**, *2*, 4812.
(51) Zecchina, A.; Bordiga, S.; Spoto, G.; Damin, A.; Berlier, G.; Bonino, F.; Prestipino, C.; Lambertim, C. *Top. Catal.* **2002**, *21*, 67.
(52) Wyckoff, R. W. G. *Crystal Structures*; Interscience: John Wiley & Sons: 1963; Vol. 1.
(53) Bandyopadhyay, M.; van den Berg, M. W. E.; Grünert, W.; Birkner, A.; Li, W.; Schüth, F.; Gies, H. *Microporous Mesoporous Mater.*, submitted.

indicate Ti incorporation inside MCM-48. Pore volume and pore diameter decrease with titanium content; however, surface area increases for low loading of titania because of additional surface of the nanoparticles deposited inside the pores. The blue shift of the absorption of TiO_2 in UV−visible spectra indicates the formation of quantum-sized titania particles. The transition shifts toward higher wavelength from first to third impregnation which is one of the evidences of the increase of cluster size with successive loading by metal oxide. XANES spectra yield 5−6-fold coordination for Ti in TiO_2/MCM-48 and show resemblance of the spectra with rutile. From EXAFS, we conclude that the structure of the nanoparticle is highly disordered after the first loading; however, successive uptake of titania leads to a local order with more than one type of coordination sphere, including a resemblance to rutile. As shown in this study, only the combination of various bulk and surface analytical techniques provides a most complete picture of the nature of the composite material.

Acknowledgment. This work has been supported by the Deutsche Forschungsgemeinschaft in the frame of the Sonderforschungsberich "Metal-support interactions in heterogeneous catalysis", SFB 558.

CM0484854